Chapter 10

Surface-Enhanced Raman Spectroscopy Characterization of Pristine and Functionalized Carbon Nanotubes and Graphene

Sabina Botti, Alessandro Rufoloni,
Tomas Rindzevicius and Michael Stenbæk Schmidt

Additional information is available at the end of the chapter

http://dx.doi.org/10.5772/intechopen.74065

Abstract

Carbon nanotubes (CNTs) and graphene are at the center of a significant research effort due to their unique physical and chemical properties, which promise high technological impact. For the future development of all the foreseen applications, it is of particular interest the study of binding interactions between carbon nanostructures and functional groups. An appropriate method is the surface-enhanced Raman spectroscopy (SERS), which provides a large amplification of Raman signals when the probed molecule is adsorbed on a nanosized metallic surface. In this chapter, we present a review of principal results obtained applying SERS for the characterization of pristine and functionalized CNTs and graphene. The obtained results encourage us to consider SERS as a powerful method to obtain a rapid monitor of the procedures used to interface graphene and nanotubes.

Keywords: carbon nanotubes, graphene, functionalization process, SERS

1. Introduction

Carbon nanotubes (CNTs) and graphene are at the center of a significant research effort due to their unique physical and chemical properties, which promise high technological impact. For the future development of all the foreseen applications, it is of particular interest the study of binding interactions between carbon nanostructures and functional groups [1–3]. Indeed,

the ability to engineer the electrical, optical, sensing, and dispersion properties of graphene and CNTs by chemical functionalization is widening considerably their potential applications generating a vast and yet largely unexplored family of carbon nanostructures for the realization of devices with novel functionalities. This task is highly challenging and the achievement of a procedure that enables a high density of functional groups, with little or no damage to the carbon structure, is of prime importance as the development of a nondestructive technique that can fully characterize the structure of functionalized graphene and CNTs.

Since long time, Raman spectroscopy has been considered as one of the most powerful tool for the characterization of carbon-based materials (see Section 2); however, Raman features associated with functional groups are usually often not observed in the Raman spectra of nanotubes and graphene due to the small quantity of the molecules attached to the carbon lattice.

In our studies, we have used the surface-enhanced Raman spectroscopy (SERS), which provides a large amplification of Raman signal when the probed molecule is adsorbed on nanosized metallic surface [4, 5]. Since the SERS effect increases by decreasing the distance between the nanostructure and the adsorbed molecule, by depositing CNTs/graphene as dilute dispersions on SERS active substrates, the Raman signal from the molecular groups deriving from functionalization/synthesis process and bound to the carbon surface, can be amplified. As a consequence, the spectral features of functional groups, otherwise very difficult to see, were recorded in the SERS spectra.

Here, we present a review of principal results obtained by applying SERS for the characterization of pristine and functionalized graphene and multiwalled nanotubes (MWNTs). The obtained results encourage us to consider SERS as a powerful method to obtain a rapid monitor of the procedures used to interface graphene and nanotubes with functionalizing groups.

2. Raman spectroscopy

In **Figure 1**, the Raman spectra of graphite (HOPG, Cree Corporation, USA), multilayer graphene, single-walled carbon nanotubes (SWNTs), double-walled nanotubes (DWNTs), and MWNTs in the range 100–2100 cm^{-1} are reported. All the samples that we used were commercially available.

The pristine SWNTs, DWNTs, and MWNTs were grown by catalytic carbon vapor deposition process, with the following characteristic: SWNTs (Nanointegris, USA, selected semiconductor) average diameter: 1.2–1.7 nm, length: 300 nm to 5 μm; DWCNTs (Nanocyl, Belgium) average outer diameter of 3.5 nm, length between 1 and 10 μm, and specific surface area of 500 m^2/g; MWNTs (Nanocyl, Belgium) average diameter: 9.5 nm, average length: 1.5 μm. We used graphene powders with particles consisting of aggregates of platelets with diameter of about 2 μm, thickness less than 5 nm, and average surface area 750 m^2/g (grade C particles, XG Sciences Inc., USA).

http://dx.doi.org/10.5772/intechopen.74065

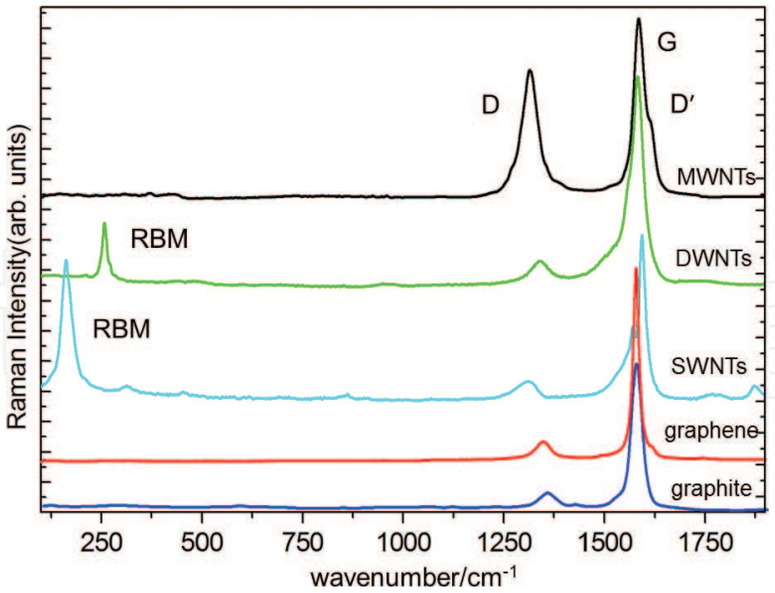

Figure 1. Raman spectra of different carbon forms: graphite, graphene, SWNTs, DWNTs, and MWNTs. The spectra were excited at 785 nm.

The Raman spectrum of graphite and its derivatives has two main peaks assigned to the first order D (1320 cm^{-1}) and G modes (1580 cm^{-1}) [6–12]. Second-order Raman spectra of carbon-based materials, and particularly of graphene, are dominated by 2D (G′) band at ~2700 cm^{-1}, caused by the existence of double electron-phonon resonance mechanism, thus making it possible to study the structure of electron bands from the analysis of resonance Raman spectra. The band has a double peak in graphite and a single peak in graphene. Both the intensity ratio I_{2D}/I_G and the shape analysis of 2D peak have been used to distinguish mono from bi or multilayer graphene [12, 13].

The D mode (A_{1g} symmetry) can be described as an in-plane breathing vibration of aromatic ring in which the six atoms move away from the center of the Brillouin zone. This band is forbidden in perfect graphitic lattice and it becomes active in the presence of disorder and deviations from an ideal structure. The G mode (E_{2g} symmetry) is due to the in-plane stretching vibration of carbon atoms pairs in which each atom moves vibrating tangentially against the other. This mode is always allowed and it is characteristic not only of graphitic rings but also of all the sp^2 structures. The ratio of D and G band intensities provides a way to estimate the amount of defects in graphitic structure, being inversely proportional to the size of ordered sp^2 domain size through the relation: $L = (2.4 \times 10^{-10}) \cdot \lambda_L^4 \cdot (I_D/I_G)^{-1}$, where λ_L is the wavelength of laser that excites the Raman spectra [9, 11, 12].

The Raman spectra of SWNTs display peculiar features as the radial breathing mode (RBM), and the double peak splitting of the G band. The frequency ω of RBMs is inversely proportional to the value of tube diameter d following the Bandow relation: [13, 14]

$$\omega = \alpha/d \tag{1}$$

where the parameter α is experimentally determined.

The optical transitions of SWNTs can be identified as inter-band transitions between the Van Hove singularities in the 1D electronic density of states (DOS) [14, 15]. The singularities are spikes in the DOS, which occur at specific energies, depending on the nanotube diameter and chirality. From band structure calculations, approximate relations were deduced between the energy *E* of inter-band transitions between DOS singularities and the nanotube diameter, suggesting that the optical absorption peaks should move to higher energy at decreasing nanotube diameter. As the nanotube diameter increases, the singularities move closer together, whereas for small diameter nanotubes, the "spikes" in the DOS are well-separated, especially near the Fermi energy and can provide initial or final states or both for a highly resonant Raman scattering process. The energy of these optical transitions are in the visible range, near to the wavelength of the most commonly used laser for excite Raman scattering. When the laser energy matches the energy difference between spikes for a particular nanotube diameter, the corresponding RBM will dominate the Raman trace. Therefore, the Raman scattering in small diameter SWNTs is diameter selective as direct consequence of the 1D electronic quantum-confinement in small diameter SWNTs.

The nanotube curvature results in different force constants for atomic displacements along the nanotube axis compared to those in the circumferential direction, causing the separation of G peak in two components, G^+ and G^- [13–17]. Differently, in the Raman spectra of MWNTs, which can be considered as an ensemble of concentric SWNTs with increasing diameters, the G peak splitting is both small and smeared out, leading to a broad G band line shape. The higher energy mode that appears as a shoulder in MWNT Raman trace is the D′ band, which is due to the same tangential vibrations of the G mode, but involving external layers that are not sandwiched between two other layers. As the D band, D′ is a double resonance Raman mode, induced by disorder and/or defects on the side walls of CNTs or ion intercalation between graphitic sheets. Indeed, this band is not observed in graphite, but it has a high intensity in intercalated graphite compounds [18].

As it will be discussed in Section 6, since less information is available on the structure of functional groups attached to the tube walls or basal plane of graphene, in our studies, we have used the SERS technique to record the Raman signal of functional groups and prove experimentally their linkage to the CNT walls.

3. Surface-enhanced Raman spectroscopy

The surface-enhanced Raman scattering (SERS), discovered three decades ago, is used to provide a drastic amplification of the Raman signal [4, 5]. The Raman signal amplification is observed when the molecule to be studied is adsorbed on a nanostructured metallic surface and the frequency of incident radiation overlaps the resonant frequency of conduction electrons in the metals. In this case, the incident electric field produces collective oscillations of metal electrons, which in turn generate a large electromagnetic field. This field is superimposed to the incoming field giving rise to its enhancement. Theoretical studies demonstrate that the induced field is particularly intense near sharp tips, interstitial crevices, and more generally, in between adjacent metal nanostructure if the distance is of few nanometers [4, 5, 19].

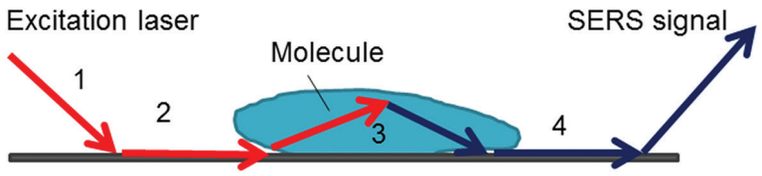

Figure 2. Scheme of SERS process steps.

However, the electromagnetic mechanism does not explain why the enhancement factor of a surface depends on the chemical nature of the adsorbed molecule [19, 20], therefore, it was hypothesized that an additional enhancement is provided by an increase of molecule polarizability due to a deformation of the distribution of the electron cloud or to the formation of resonant charge transfer complex between the metal and the adsorbed molecule.

We can then summarize the SERS process steps, depicted in **Figure 2**: (1) the incident laser impinges on nanostructured metallic surface, (2) plasmons excitation with electric field amplification, (3) Raman scattered light emission, and (4) Raman scattered light transferred back to plasmons and scattered in air. The surface enhancement effect is so pronounced because the Raman signal enhancement occurs twice.

4. SERS substrates

To be used in a sensor system, a SERS substrate should enhance the Raman effect sufficiently to enable consistent and uniform chemical detection sensitivity across the surface, maintaining its properties as long as possible in the time and to provide a high number of sites for molecular adsorption.

In principle, all systems possessing free carriers show the surface enhancement effect. However, the plasmon properties—such a wavelength and width of its resonance—depend on the nature of the metal surface and on its geometry and affect the enhancement factor (EF) of the surface [4, 5, 19]. The width of plasmon resonance resulted to be: $w = \gamma(\varepsilon_b + 3)$, where γ is the electron scattering rate and ε_b is the contribution to the inter-band transitions to the dielectric constant. Smaller conductivity and a large number of inter-band transitions in the region of plasmon resonance give resonance peak with large width and hence smaller amplification of electric field [19]. To this respect, the coin metals (Ag, Au, and Cu) resulted to be the most appropriate to be used for SERS with their amplification factors much larger than unity. Differently, the enhancement factor of good conductors as Al, Pt, and In is larger but not much larger than unity and is only slightly greater than unity for most other metals. The other advantage of using coin metals is that their plasmon resonance wavelength is in the visible–near infrared.

Early SERS experiments used gold colloids in solution. Nowadays, by exploiting semiconductor lithographic fabrication technology, periodic patterns on Si surface can be reproducibly fabricated over large areas. Ordered geometry provides uniform SERS signals from anywhere on the active surface, avoiding that only small uncontrolled areas of the total metal surface

Substrate	EF
Klarite™	1.1×10^6
Nanova	8.0×10^5
Technical University of Denmark	8.0×10^8

Table 1. Enhancement factors of gold coated substrates with different geometry.

have the correct geometry for surface enhancement, as occurred by using substrates with random nanosized roughening or nanoparticle separation and sharp metallic features, produced with the previous techniques. Usually, the SERS substrates are gold coated because, although the gold has a smaller EF than silver, it is more resistant against oxidation in air.

We used three variations of SERS active gold substrates: an ordered array of inverted square-based pyramids, (Klarite™, D3 Technologies Ltd3), an electrochemically nano-roughened surface (Nanova), and an array of nanopillars, 50–80 nm in width, 600 nm in height, fabricated by the Department of Micro and Nanotechnology of the University of Denmark [21–23].

We measured the EFs of all the above cited substrates by measuring the Raman signal of the same molecule, in this way only electromagnetic enhancement due to the geometry of the used structure was considered, avoiding the effect of chemical enhancement [20, 24]. The obtained results are reported in **Table 1**. The regularity of nanostructure guaranteed a uniform enhancement factor across the surface and a high reproducibility of Raman signal in spite of the differences among the EFs.

5. Sample preparation

As discussed in the previous paragraph, the field enhancement strongly decreases with the distance from the metallic surface, as consequence delivering the substance under study in close proximity of the metal surface is a prerequisite for measuring SERS signals. Therefore, the samples were analyzed as evaporated films prepared by dropping on the SERS active surface a controlled volume of a solution of CNTs or graphene in ultra-pure water (1 mg/mL). The solvent spreads across the surface selectively evaporates leaving a dried film, which is clearly visible under the optical microscope coupled with the spectrometer (see **Figure 3**).

In our procedure, the substrates were used as-received without any pre-treatment and the solvent evaporated in air without any heating.

We examined the dried film morphology under high-resolution scanning electron microscope (HR-SEM), using a Leo 1525 hot cathode field emission microscope, with a resolution of 1.5 nm at 20 kV.

The SERS activity depends either from the substrate morphology either from the number of sites in the surface that are accessible to the molecular adsorption. In fact, the SERS signal from molecules on the second monolayer and beyond is reduced because the SERS effect depends on the distance between the nanostructure and adsorbed molecule, as shown in **Figure 4**.

http://dx.doi.org/10.5772/intechopen.74065

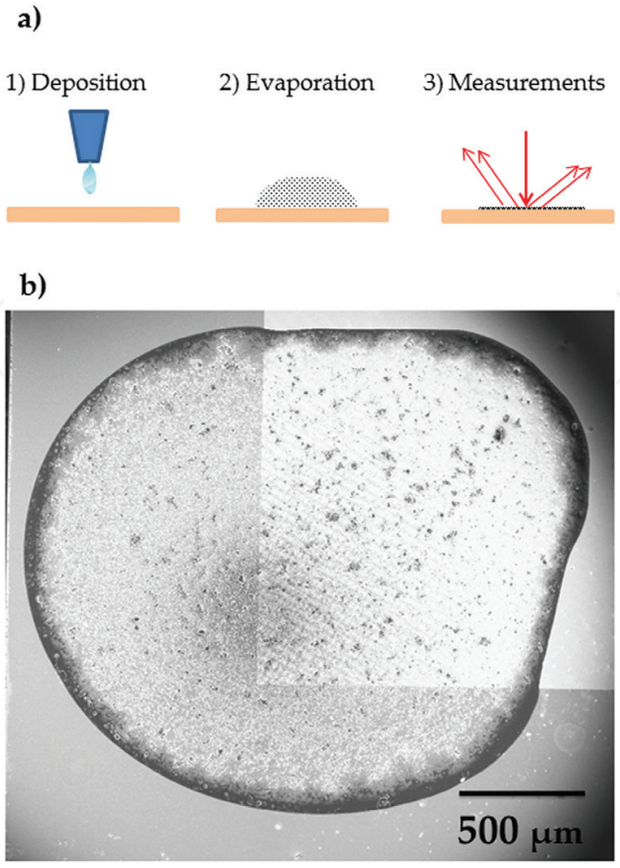

Figure 3. (a) Sequential steps of the drop and dry technique for films deposition and (b) top view of dried film.

When the number of analyte molecules is too large, a sample layer is formed covering the molecules with surface-enhanced Raman signal. To this respect, it is of prime importance that the substrate geometry provides enhancement region accessible for molecular adsorption.

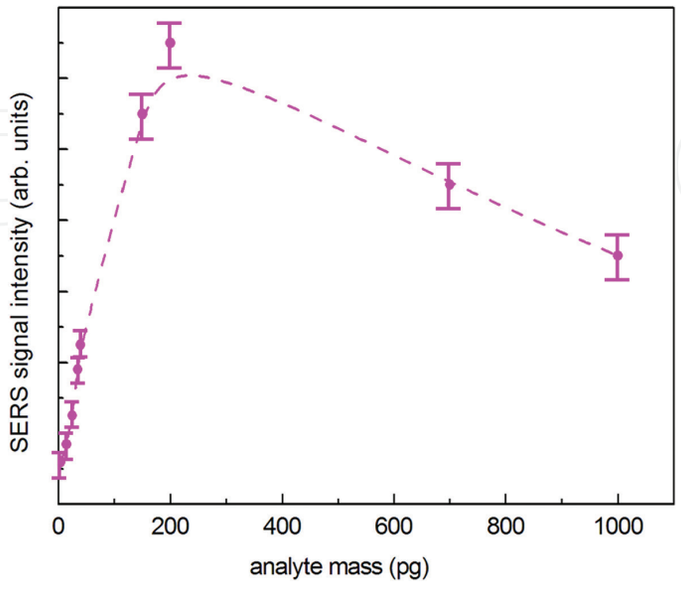

Figure 4. Variation in the intensity of surface-enhanced Raman signal with the amount of analyte mass probed by the laser.

6. Raman spectrometers

In the first steps of our works, we acquired SERS and Raman spectra using a Raman spectrometer BwTek (i-Raman 785.), equipped with a micro-positioning system for fine xyz adjustments and a video camera for sampling viewing. The system uses an air-cooled charge coupled device (CCD) detector. The 785 nm laser light, to guarantee the coupling with gold plasmons, was focused onto the sample using a 20× objective (corresponding to a laser beam diameter of 90 μm, as already mentioned). Samples were moved into position using the xyz translational stage. The Raman spectra were acquired in the wavelength range 789–1048 nm corresponding to Raman shifts of 75–3200 cm^{-1} (resolution better than 3 cm^{-1}).

Raman mapping was performed with a high-resolution micro-Raman spectrometer (Horiba Xplora) with 785 nm excitation wavelength. The Raman signal was collected through a 100× objective in the range 100–2000 cm^{-1} with accumulation time of 10 s per spectrum. Areas of the substrates up to 10 × 10 μm were scanned with an acquisition grid of 0.6 and 0.8 μm step size in x and y, respectively. All the spectra were obtained with 100 μW laser power, to avoid sample heating and damaging. The SERS maps were obtained analyzing the peak intensity of every spectrum. Raman spectra were also acquired with 532 nm excitation (range 400–3000 cm^{-1}, acquisition time 10 s).

7. Results and discussion

Controlled volumes of pristine MWNT solutions were dropped on SERS active substrates, the SERS spectra acquired in different spatial positions, maintaining all the experimental parameters unchanged are reported in **Figure 5**.

The SERS trace (a) has no significant differences in comparison of that reported in **Figure 1**, if one excepts the amplification of the signal whereas curves (b) and (c) show variations in some Raman line intensities, line shape and appearance of several sharp peaks, in the frequency range 400–1100 cm^{-1}, characteristics of C_{60}-like molecules [25].

We observed a gradual increase of the D band, which indicates an enhanced degree of disorder, with a concomitant modification of the G band profile, consisting in a peak splitting due to the increase of D′ band at its high energy side. The peak at about 250 cm^{-1} in the SERS curves (b) and (c) is similar to that at 171 cm^{-1} in Raman spectrum of SWNTs, reported in **Figure 1**.

The RBMs are not often observed in MWNTs, its observation in SERS trace is consistent with the fact that for a molecule adsorbed on a nano-structured surface, the modes which involve atoms vibrating perpendicularly to the surface are more enhanced than the others [26]. However, the observed RBM width (45 cm^{-1}) is larger than that measured in the SWNT Raman spectra [16, 17].

This finding can be explained considering that in a MWNT also the radial vibrations of outer shells contribute to this mode, producing a number of overlapping RBM peaks larger than those expected for SWNTs with the same distribution of diameter [18].

http://dx.doi.org/10.5772/intechopen.74065

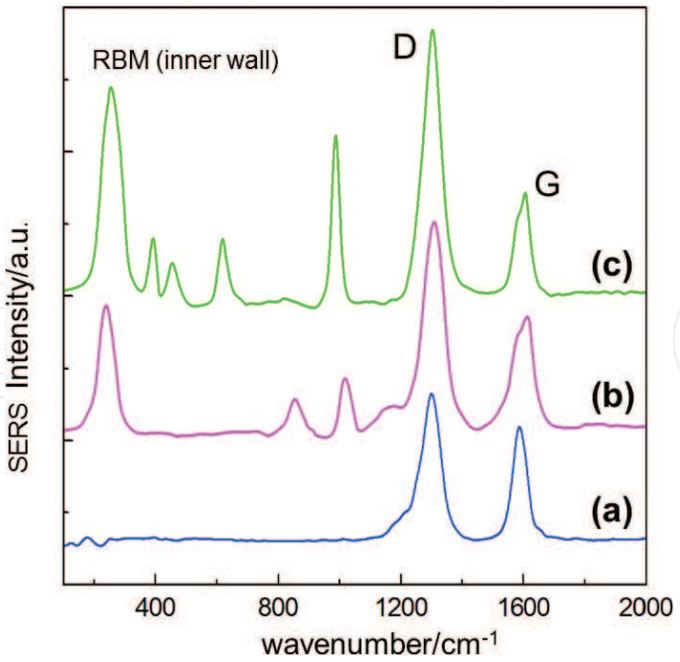

Figure 5. SERS spectra of pristine MWNT dried film. The MWNT layer thickness is decreasing from spectrum (a) to (c).

The diameter of SWNTs can be calculated from the frequency of corresponding RBM, through the Bandow relation [13–15]. Since the RBM intensity strongly decreases when the tube diameter

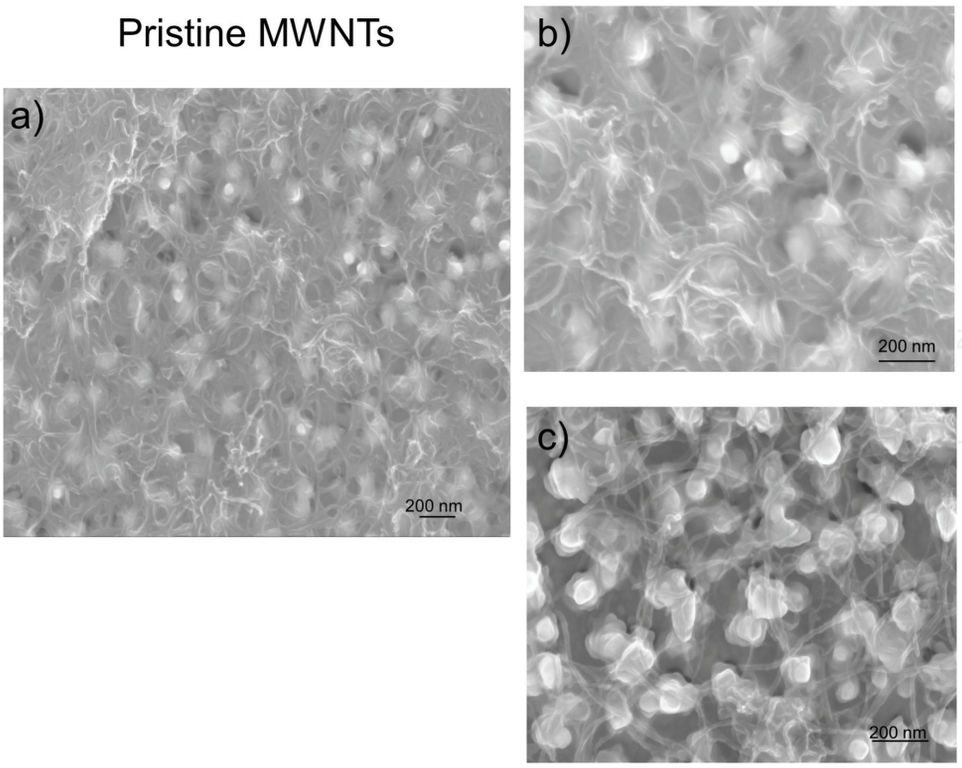

Figure 6. (a) HR-SEM image of pristine MWNT film deposited on SERS substrate. (b) Magnified view of region with larger thickness layer (c) Magnified view of region with thinner layer. The leaning effect of nanopillars is evidenced.

increases, we can roughly estimate the inner diameter of MWNTs from their RBMs in the SERS spectra by using the same rule. The RBM at 250 cm^{-1} corresponds to an inner tube diameter of 0.8 nm. These values are compatible with those reported in the data sheet of MWNTs from the manufacturer.

Figure 6 presents a HRSEM view, taken at different magnification of pristine MWNT films. The MWNTs are tightly interlaced forming a web of filaments that are distributed across the SERS active surface, occupying the regions with highest Raman signal amplification as the space between the nano-pillars. However, the layer thickness is not uniform across the deposited patch and this is reflected in the observed differences between the SERS spectra reported in **Figure 5**.

In fact, these variations can be interpreted by considering the breaking of the nanotubes into species such as amorphous carbon, tubular fragments, and closed shell fullerenes. Such reactions are of chemical nature occurring at the nanotube metal substrate interface.

Figure 7 illustrates the comparison between the Raman spectra of pristine and covalently functionalized MWNTs. The carboxyl functionalization was performed by a reflux in sulfuric/nitric acid (Nanolab, average diameter = 30 nm, length 1–5 μm, from now on denoted as COOH-MWNTs). This process leads to the concentration of COOH groups on the nanotube surface. By reacting the carboxylate CNTs with ethylene diamine, nanotubes with amide linkage and a primary amine group at the end of carbon chain are obtained (Nanolab, average diameter = 15 nm, length 1–5 μm, from now on denoted as NH_2-MWNTs). However, in the Raman spectra of covalently functionalized vibrational modes that can be directly related to molecular groups are not observed.

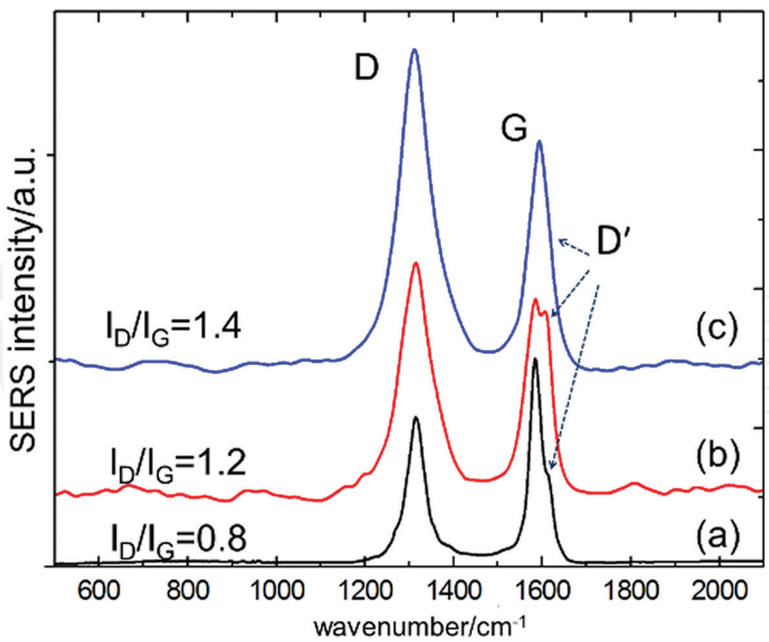

Figure 7. Raman spectra of MWNT mat. (a) Raman spectrum acquired from pristine MWNT film, I_D/I_G = 0.8; (b) Raman spectrum acquired from COOH-functionalized MWNTs, I_D/I_G = 1.2; (c) Raman spectrum acquired from NH_2-functionalized MWNTs, I_D/I_G = 1.4.

http://dx.doi.org/10.5772/intechopen.74065

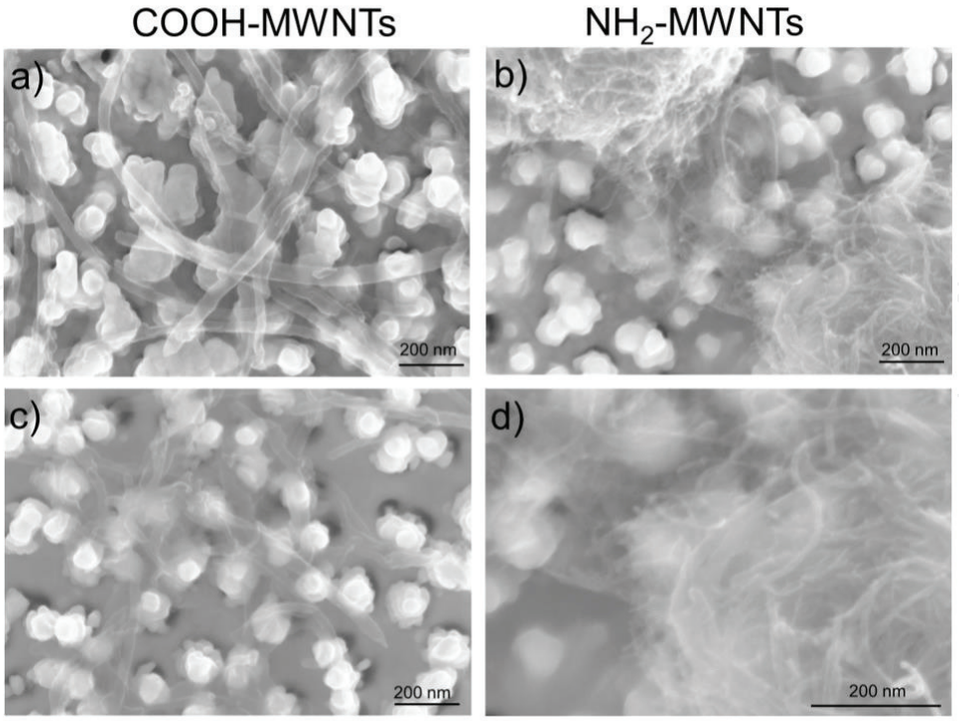

Figure 8. HR-SEM images of (a) COOH-MWNT and (b) NH_2-MWNT films deposited on SERS substrate; (c) magnified view of region (a); (d) magnified view of region (b) evidencing the formation of a dense layer.

As a consequence, the use of Raman spectroscopy to study the structure of functionalized CNTs is routinely limited to the evaluation of the I_D/I_G ratio, since the interaction between carbon nanotube wall and functional groups is expected to produce a higher density of sp^3 hybridized carbon sites, with consequent increase of I_D/I_G ratio [27–29].

However, when a set of spectra is recorded from the same pristine CNTs sample, we frequently observed a variation in the I_D/I_G ratio, up to the 15% of its average value, which is sometimes apparently of the same order as that recorded after the chemical functionalization. Although a more efficient discrimination can be reached by applying the principal component analysis [30], the observation of Raman spectral changes induced by the chemical functionalization is challenging.

In **Figure 8** are illustrated the different morphologies of functionalized MWNT-dried films. Due to the small outer diameter, the NH_2-MWNTs are tightly interlaced forming a dense web of filaments. Differently, the drying of COOH-MWNT solution forms a very thin layer with some groups of few isolated nano-tubes.

We acquired the SERS spectra from functionalized MWNT films in different spatial positions, maintaining all the experimental parameters unchanged obtaining reproducible spectra, shown in **Figure 9**.

In addition to the signal enhancement, compared to conventional Raman spectra, the SERS traces show sharp peaks in wavenumber region ascribable to vibrations of molecular groups;

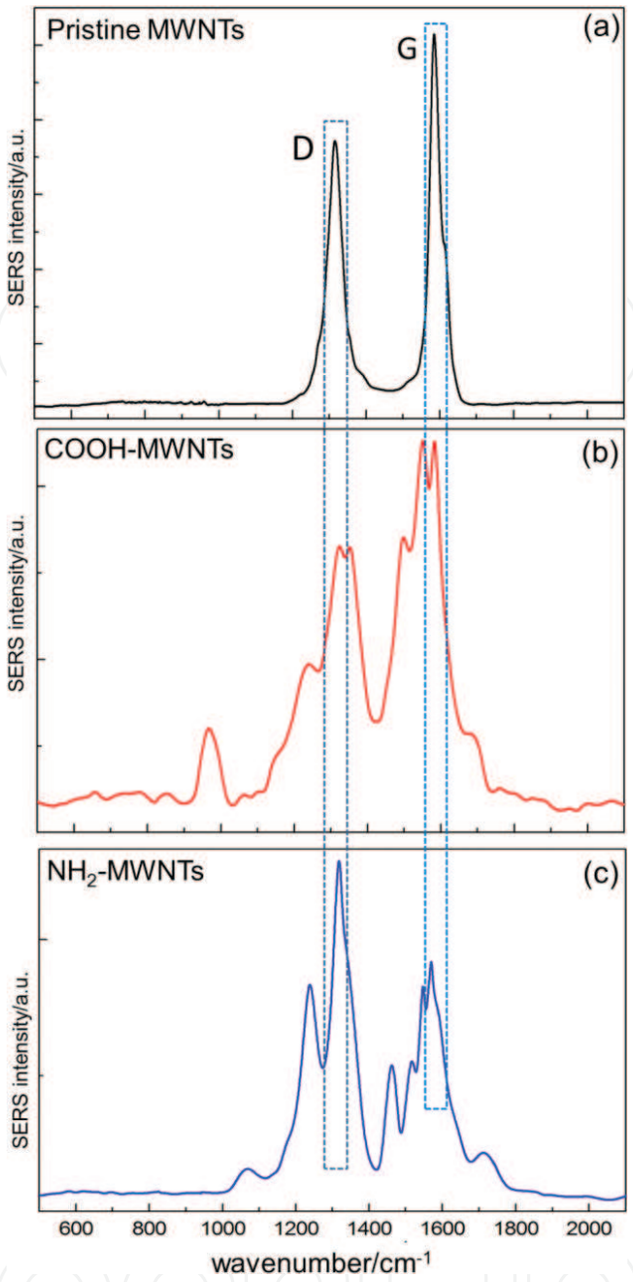

Figure 9. SERS spectra of pristine (a), COOH-MWNTs (b), and NH_2-MWNTs (c).

namely the C—O—C stretching (shoulder at around 1260 cm^{-1}), CH_3 deformation (1320 cm^{-1}), C—N stretching (1240 cm^{-1}, 1460 cm^{-1}), and C═O stretching at 1730 cm^{-1} [31, 32]. The presence of these bands proves experimentally the linkage of desired molecular groups to the nanotube walls. It is worth to note that the C═O stretching appears in both covalently functionalized samples owing to the functionalization procedure, which introduces the linkage of amides after that of carboxylate.

In the SERS spectrum of COOH-MWNTs, the D′ band is not distinguishable as shoulder next to the G band, indicating that this sample has a lower amount of defects, as expected for carbon nanotubes with large diameter, which exhibit reduced tip curvature and in turn fewer

http://dx.doi.org/10.5772/intechopen.74065

structural defects. It is worth to note that because there is no shift between SERS bands and the corresponding ones in the Raman spectrum, the interaction between MWNTs and the active surface is physical.

We can note also that in the SERS spectra of functionalized MWNTs, shoulders of G band at 1510 and 1544 cm^{-1} are clearly distinguishable. Although in the SERS trace of NH_2-MWNTs, the presence of the latter peak could be ascribed to the combination of N-H bend and C-N stretch, since these bands appear in both functionalized samples, they were assigned to disordered carbon with sp^3 bonds. In fact, the peak at 1510 cm^{-1} was observed in carbon with sixfold rings and rings with other orders, whereas the higher frequency peak, was often recorded in amorphous hydrogenated carbon, due to the C—C bond strain caused by the formation of C—H covalent bonds [6, 7, 9, 11, 33].

Surprisingly, also in the SERS spectra of pristine graphene, we recorded a large number of sharp peaks belonging to molecular group vibrations, as illustrated in **Figure 10**: namely C—C=O bending (520–570 cm^{-1}), C—O—C deformation, (850 cm^{-1}), O—H (900–960 cm^{-1}) and CH_2 (1040 cm^{-1}) bending, and C—C(O)—C stretching 1180–1270 cm^{-1}) [31, 34].

Functional groups as ethers, carbonyls, carboxyls, and hydroxyls are likely retained in the graphene structure, as a consequence of chemical exfoliation process and the presence of oxygen and hydrogen atoms in few at percentage was confirmed by XPS measurements of manufacturer [35].

We can also note that close to the G band are present the peaks of disordered carbon already observed in functionalized MWNTs. The presence of disordered carbon peaks in the SERS

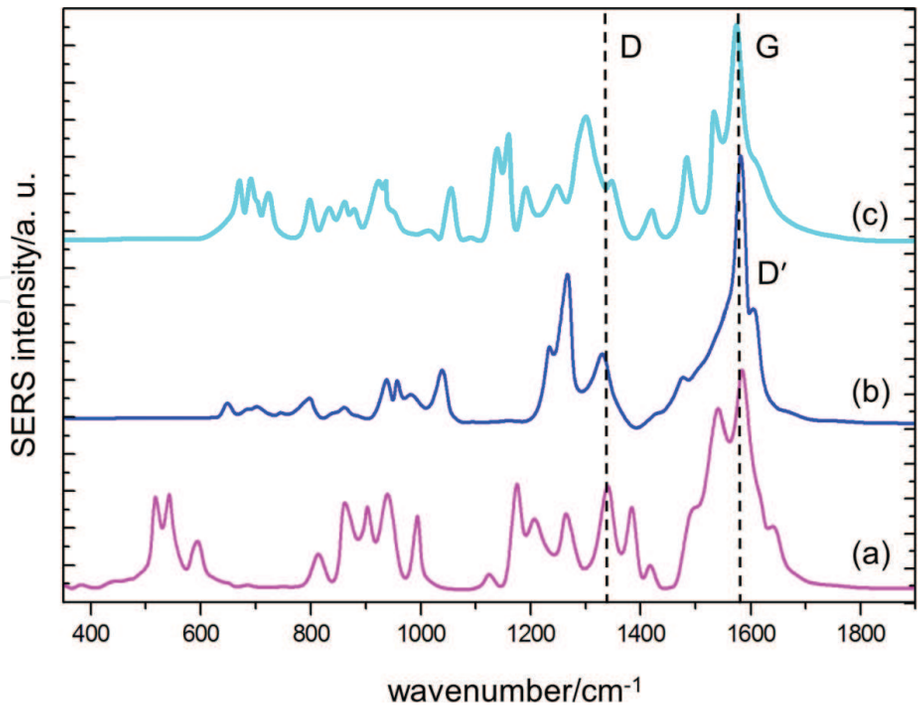

Figure 10. SERS spectra of pristine graphene. The spectra (a), (b), and (c) were acquired at different scanning positions across the dried film.

spectra of graphene and functionalized MWNTs is a further proof of evidence of the formation of tetrahedrally coordinated bonds between carbon atoms and molecular groups.

We acquired SERS spectra for each point of a selected area of pristine graphene films with a high-resolution micro-Raman spectrometer (Horiba Xplora) (see **Figure 11**). The areas were scanned with an acquisition grid of 0.6 and 0.8 μm in x and y, respectively. We selected the wavenumber region 500–1280 cm^{-1} to represent the functional groups concentration and we constructed the SERS images, illustrated in **Figure 11(b)** and **(d)**, plotting the intensity of the peaks located in this region.

Optical images show significant variation in the dried film thickness along the scanned area, due to a poor dispersibility of pristine graphene in the distilled water. However, the SERS signal is always detectable with good spectral reproducibility and an intensity variation much smaller than that expected, considering that the SERS signal from the second monolayer and beyond is strongly reduced. This finding further confirms that the functional groups are distributed at the edges of graphene structure: the larger thickness and hence the weaker enhancement experienced by the molecular groups, can be compensated by a higher concentration.

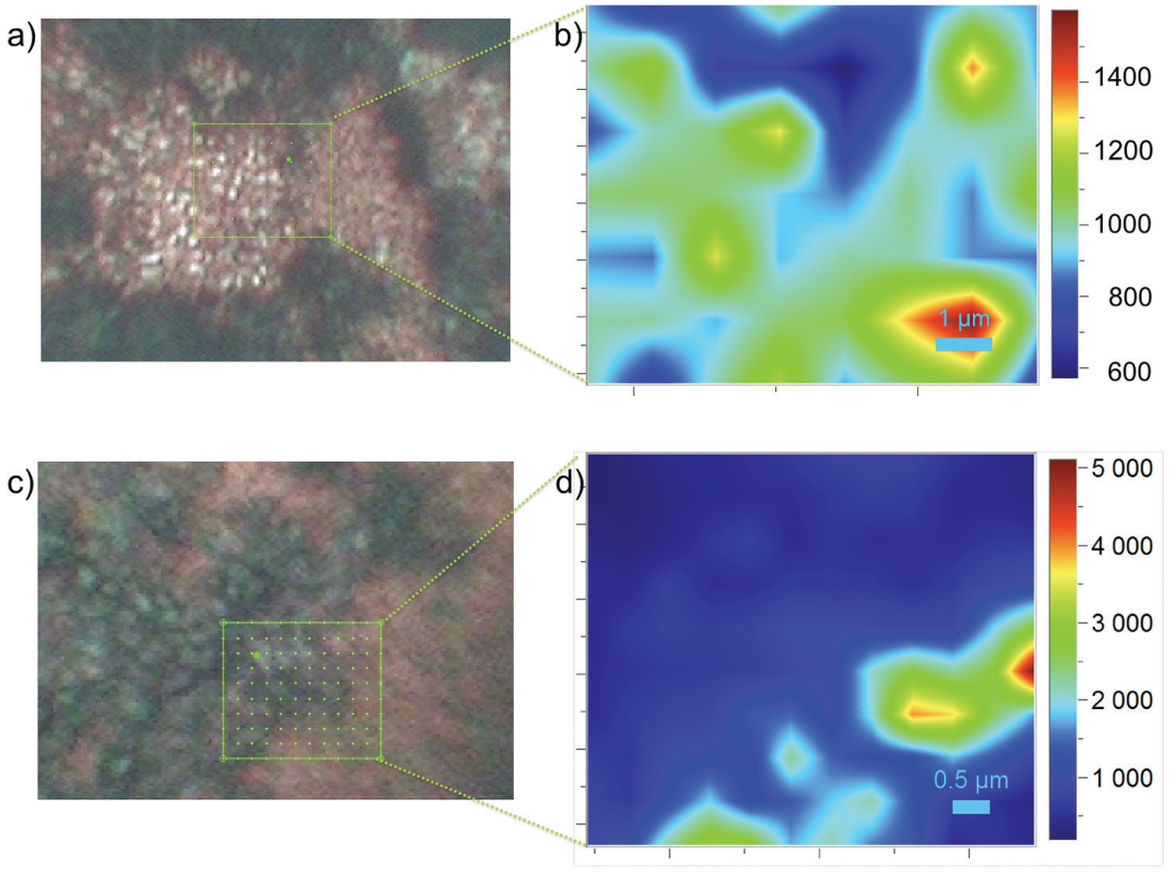

Figure 11. (a) Image of pristine graphene dried film, acquired with the optical microscope coupled with the Raman spectrometer; the green rectangle indicates the region selected to acquire the map (b). (c) and (d) represent the same for another region of the substrate. The visualization of Raman maps is obtained by using as contrast parameters the intensity of functional group peaks.

http://dx.doi.org/10.5772/intechopen.74065

8. Conclusions and outlook

In summary, we performed SERS measurements on graphene pristine and functionalized MWNTS and graphene nano-structured film deposited on gold-coated Si nano-pillar substrates. The strong surface enhancement effect allowed us to record the Raman signal from functional molecules that are not recorded in conventional Raman spectra proving experimentally their linkages to the CNT walls and graphene edges. By using the relative intensities of specific SERS features as contrast parameters to obtain SERS maps, it is possible to study the distribution of functional groups across the scanned area.

The obtained results encourage us to consider SERS as a powerful method to obtain a rapid monitor either of the procedures used to interface graphene and nanotubes with functionalizing groups either of synthesis process of graphene as chemical exfoliation.

Author details

Sabina Botti[1]*, Alessandro Rufoloni[1], Tomas Rindzevicius[2] and Michael Stenbæk Schmidt[2]

*Address all correspondence to: sabina.botti@enea.it

1 Fusion and Nuclear Security Department, ENEA, Frascati, Italy

2 Department of Micro and Nanotechnology, Technical University of Denmark, Lyngby, Denmark

References

[1] Hersam MC. Progress towards monodisperse single-walled carbon nanotubes. Nature Nanotechnology. 2008;**3**:387-394. DOI: 10.1038/nano.2008.135

[2] Byrne MT, Gun'ko YK. Recent advances in research on carbon nanotube-polymer composites. Advanced Materials. 2010;**22**:1672-1688

[3] Kim SW, Kim T, Kim YS, Choi HS, Lim HJ, Yang SJ, Park CR. Surface modifications for the effective dispersion of carbon nanotubes in solvents and polymers. Carbon. 2012;**50**:3-33

[4] Jeanmaire DL, Van Duyne RP. Surface Raman spectro-electrochemistry. Journal of Electroanalytical Chemistry. 1977;**84**:1-20

[5] Haynes CL, McFarland AD, Van Duyne RP, Surface-enhanced Raman spectroscopy. Analytical Chemistry. 2005;**77**:338A-346A and references therein

[6] Ferrari AC. Raman spectroscopy of graphene and graphite: Disorder, electron-phonon coupling, doping and non-adiabatic effects. Solid State Communications. 2007;**143**:47-57

[7] Ferrari AC, Basko DM. Raman spectroscopy as a versatile tool for studying the properties of graphene. Nature Nanotechnology. 2013;**8**:235-246

[8] Malard LM, Pimenta MA, Dresselhaus G, Dresselhaus MS. Raman spectroscopy in graphene. Physics Reports. 2009;**473**:51-87

[9] Casiraghi C, Hartschuh A, Qian H, Piscanec S, Georgi C, Fasoli A, Novoselov KS, Basko DM,Ferrari AC. Raman spectroscopy of graphene edges. Nano Letters. 2009;**9**:1433-1441

[10] Tuinstra F, Raman KJL. Spectra of graphite. The Journal of Physical Chemistry. 1970;**53**(3): 1126-1310

[11] Jiang J, Pachter R, Mehmood F, Islam AE, Maruyama B, Boeckl JJ. A Raman spectroscopy signature for characterizing defective single-layer graphene: Defect-induced I(D)/I(D′) intensity ratio by theoretical analysis. Carbon. 2015;**90**:53-62

[12] Lucchese MM, Stavale F, Ferreira EHM, Vilani C, Moutinho MVO, Kapaz RB, Achete CA. Quantifying ion-induced defects and Raman relaxation length in graphene. Carbon. 2010;**48**:1592-1597

[13] Rao AM, Richter E, Bandow S, Chase B, Eklund PC, Williams KA, et al. Diameter-selective Raman scattering from vibrational modes in carbon nanotubes. Science. 1997;**275**:187-191

[14] Bandow S, Asaka S, Saito Y, Rao AM, Grigorian L, Richter E, Eklund PC. Effect of the growth temperature on the diameter distribution and chirality of single-wall carbon nanotubes. Physical Review Letters. 1998;**80**:3779-3782. DOI: 10.1103/PhysRevLett.80.3779

[15] Dresselhaus MS, Dresselhaus G, Jorio A, Souza Filho AG, Saito R. Raman spectroscopy on isolated single wall carbon nanotubes. Carbon. 2002;**40**:2043-2061

[16] Botti S, Ciardi R, Terranova ML, Piccirillo S, Sessa V, Rossi M. Carbon nanotubes and nanowires grown from spherical carbon nano-particles. Chemical Physics Letters. 2002;**355**:395-399

[17] Botti S, Ciardi R, Terranova ML, Piccirillo S, Sessa V, Rossi V-AM. Self-assembled carbon nanotubes grown without catalyst from nanosized carbon particles adsorbed on silicon. Applied Physics Letters. 2002;**80**:1441-1443

[18] Lehman JH, Terrones M, Mansfield E, Hurst KE, Meunier V. Evaluating the characteristics of multiwall carbon nanotubes. Carbon. 2011;**49**:2581-2602

[19] Le Ru E, Etchgoin P. Principles of Surface-Enhanced Raman Spectroscopy and Related Plasmonic Effects. Elsevier Science; 2008 ebook ISBN: 9780080931555 and references therein

[20] Botti S, Cantarini L, Almaviva S, Puiu A, Rufoloni A. Assessment of SERS activity and enhancement factors for highly sensitive gold coated substrates probed with explosive molecules. Chemical Physics Letters. 2014;**592**:277-281

[21] Schmidt MS, Hübner J, Boisen A. Large area fabrication of leaning silicon nano-pillars for surface enhanced Raman spectroscopy. Advanced Materials. 2012;**24**(10):OP11-OP18

[22] Yang J, Palla M, Bosco FG, Rindzevicius T, Alstrøm TS, Stenbæk Schmidt M, Boisen A, Ju J, Lin Q. Surface-enhanced Raman spectroscopy based quantitative bioassay on aptamer-functionalized nanopillars using large-area Raman mapping. ACS Nano. 2013; **7**(6):5350-5359

[23] Wu K, Rindzevicius T, Stenbæk Schmidt M, Bo Mogensen K, Hakonen A, Boisen A. Wafer-scale leaning silver nanopillars for molecular detection at ultra-low concentrations. Journal of Physical Chemistry C. 2015;**119**(4):2053-2062

[24] Botti S, Cantarini L. Unpublished data

[25] Dresselhaus MS, Dresselhaus G, Eklund PC. Raman scattering in fullerenes. Journal of Raman Specroscopy. 1996;**27**:351-371

[26] Moskovits M. Surface selection rules. The Journal of Chemical Physics. 1982;**77**:4408-4416

[27] Osswald S, Havel M, Gogotsi Y. Monitoring oxidation of multiwalled carbon nanotubes by Raman spectroscopy. Journal of Raman Specroscopy. 2007;**38**:728-736

[28] Lefrant S, Baltog I, Baibarac M, Mevellec JY, Chauvet O. SERS studies on single-walled carbon nanotubes submitted to chemical transformation with sulfuric acid. Carbon. 2002;**40**(12):2201-2211

[29] Graupner R. Raman spectroscopy of covalently functionalized single-wall carbon nanotubes. Journal of Raman Specroscopy. 2007;**38**:673-683

[30] Sato-Berrù RY, Basiuk EV, Saniger JM. Application of principal component analysis to discriminate the Raman spectra of functionalized multiwalled carbon nanotubes. Journal of Raman Specroscopy. 2006;**37**:1302-1306

[31] Lin-Vien D, Colthup N, Fateley W, Grasselli J. The Handbook of Infrared and Raman Characteristic Frequencies of Organic Molecules. 1st ed. London: Academic Press, Elsevier; 1991. ISBN: 9780080571164

[32] Ramanathan T, Fisher FT, Suoff RS, Brinson LC. Amino-functionalized carbon nanotubes for binding to polymers and biological systems. Chemistry of Materials. 2005;**17**: 1290-1295

[33] Ferrari AC, Robertson J. Interpretation of Raman spectra of disordered and amorphous carbon. Physical Review B. 2000;**61**(20):14095-14107

[34] Botti S, Rufoloni A, Laurenzi S, Gay S, Rindzevicius T, Schmidt MS, Santonicola MG. DNA self-assembly on graphene surface studied by SERS mapping. Carbon. 2016;**109**: 363-372

[35] XG Sciences grade C particle data sheets

IntechOpen